# UC Davis
## UC Davis Previously Published Works

**Title**

Preparation of Activated Carbon and Silica Particles from Rice Straw

**Permalink**

https://escholarship.org/uc/item/67p8r1k8

**Journal**

ACS Sustainable Chemistry & Engineering, 2(4)

**ISSN**

2168-0485

**Authors**

Hu, Sixiao
Hsieh, You-Lo

**Publication Date**

2014-04-07

**DOI**

10.1021/sc5000539

Peer reviewed

# ACS Sustainable Chemistry & Engineering

# Preparation of Activated Carbon and Silica Particles from Rice Straw

Sixiao Hu[†] and You-Lo Hsieh*,[†]

[†]Fiber and Polymer Science, University of California, Davis, One Shields Avenue, Davis, California 95616, United States

**S** *Supporting Information*

**ABSTRACT:** An efficient three-step process using toluene/ethanol, $NaClO_2$, and KOH has been successfully devised to isolate pure cellulose from rice straw while generating two filtrates as activated carbon and silica precursors. The $NaClO_2$ dissolution filtrate contains oxidized lignin and hemicellulose as carbon precursors as well as sodium carbonates as activating agents for direct carbonization (800 °C) into highly porous ($0.90 \ cm^3/g$), high specific surface area ($997 \ m^2/g$), activated carbon particles (100−500 nm). The KOH dissolution filtrate contains mainly potassium silicate that could be precipitated by dilute acidified poly(ethylene oxide) and calcined (500 °C) to pure, uniformly sized (100−120 nm), nonporous silica nanospheres. Deriving these additional activated carbon and silica particles along with nanocellulose creates advance materials while fully utilizing all major components in rice straw, the highest quantity agricultural crop byproduct in the world.

**KEYWORDS:** *Activated carbon, Porous, Monodispersed silica, Green chemistry, Rice straw utilization,*
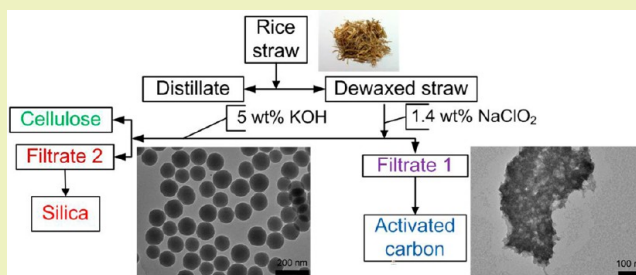
## ■ INTRODUCTION

Lignocellulosic biomass, such as agricultural crop residues, forestry byproducts, and municipal waste, is a rich source of renewable energy and materials. Lignocellulosic materials have been converted to biofuel such as ethanol,[1−3] hydrogen, and other combustible gases,[4,5] as well as nanocellulose,[3−5] carbon,[2,5] and silicon-based[6,7] materials. Cellulose nanocrystals and nanofibrils have been isolated from various major agricultural residuals including rice straw,[6] wheat straw, and soy hulls.[7] Direct thermal processing of various biomass has also generated charcoals,[4] activated carbon,[8] and silicon-based advanced materials including mesoporous silica[9] as well as silicon carbide and nitride.[10] Simultaneous derivation of parallel products from specific biomass for full utilization has not been given much attention.

Rice straw represents the largest agricultural byproduct around the world. Rice is the largest cereal crop and the highest valued agricultural commodity ($187 billion in 2011) in the world.[11] Although third in quantity (723 million MT in 2011) behind sugar cane and maize, rice production generates the highest quantity of byproduct as rice straw accounts from 1 to 1.5 kg per kg of rice grain harvested.[12] Direct use has presented some shortcomings as rice straw is a marginal feed compared with other cereal straw and causes severe furnace fouling and ash production when burned to produce steam.

Other utilization of rice straw has mainly involved single product development by converting certain components while removing others employing biochemical, chemical, and/or thermal processes. Ethanol production was improved by enzymatic saccharification of cellulose and hemicellulose,[13] while hydrogen-rich gas production was made efficient via microwave-assisted pyrolysis of rice straw.[14] Long, highly crystalline, cellulose fibers have been extracted from rice straw via alkali and enzymatic methods.[15] Activated carbons were prepared from rice straw by KOH activation and carbonization at 800−900 °C[16,17] or preoxidation at 200 °C and $(NH_4)_2HPO_4$ activation at 700 °C[18] to reach 1900 and 1150 $m^2/g$ specific surface areas, respectively, comparable to commercially available activated carbon products. Silica nanospheres were prepared from alkali dissolution of burned straw ashes and then acid precipitation[19] to better control nanoparticle sizes from 16 to 100 nm.[20] Uniform nanodisks were also prepared by sulfuric acid precipitation of dissolved silica from rice straw ashes, followed by freeze-drying.[21] Silicon carbide and nitride nanorods were fabricated by direct pyrolysis of rice straw under nitrogen from 1400 to 1800 °C.[22]

The significant lignocellulosics, that is, 32−47% cellulose, 19−27% hemicellulose, and 5−24% lignin, as well as 7−20% silica and trivial amount of waxes and minerals in rice straw[20,23−27] present opportunities for simultaneous development of multiple products. We have developed a simple approach to isolate cellulose, lignin/hemicelluloses, and silica components in rice straw with minimal chemical and energy input.[6] Pure cellulose was extracted from rice straw via an efficient $NaClO_2$−KOH process with at least 36% yield, where dewaxing in 2:1 v/v toluene/ethanol extraction was followed by lignin removal via acidified $NaClO_2$ and then hemicellulose and silica isolation by KOH. Cellulose nanocrystals and nanofibrils have been derived from pure rice celluloses via sulfuric acid hydrolysis[6,28] and 2,2,6,6-tetramethylpyperidine-1-oxyl (TEMPO)-mediated oxidation,[28] respectively, and then assembled into fibrous and porous matrixes.

 **A**
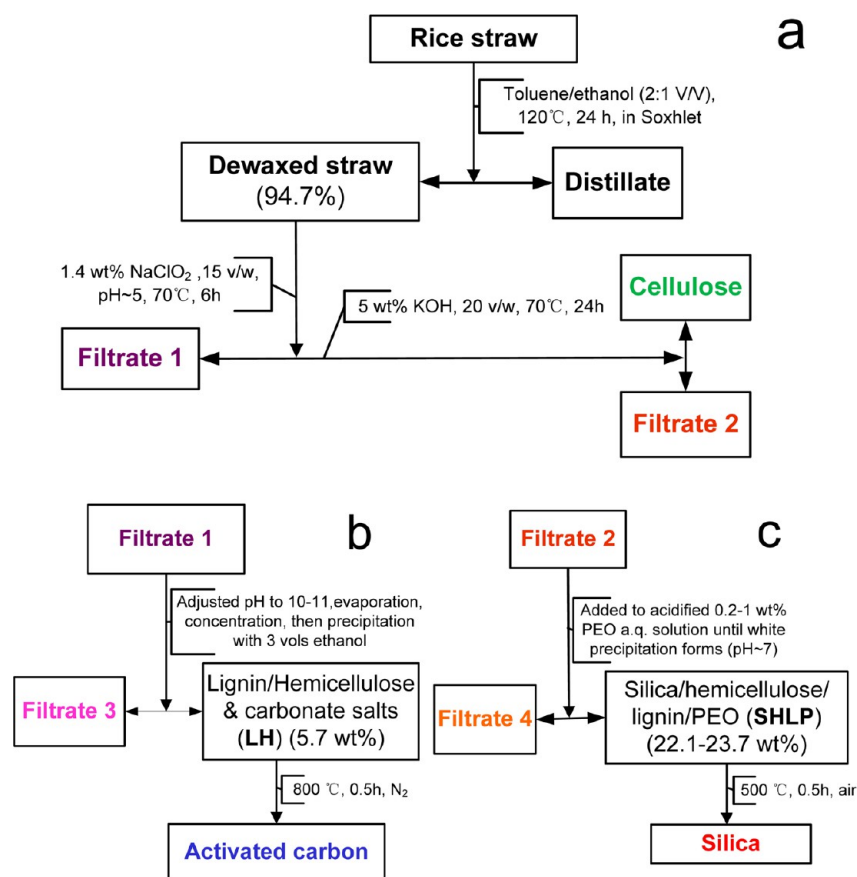
**Figure 1.** Scheme for (a) isolation of celluloses, lignin-rich filtrate 1, and silica-rich filtrate 2 from rice straw; (b) activated carbon from filtrate 1; and (c) silica from filtrate 2.

The goal of this work was to develop additional advanced materials from the as-derived extracts of two dissolution streams in isolating pure cellulose toward utilization of all major rice straw components, that is, lignin, hemicelluloses, and silica. $NaClO_2$ and KOH were used as the former is a strong oxidant that could break the strong bonding among the lignocellulosics, and the latter could dissolve silica in rice straw. The $NaClO_2$ dissolution stream from the dewaxed rice straw contains oxidation products of lignin and hemicellulose as well as sodium byproducts. As lignin and hemicelluloses were intrinsically bound to each other and thus very difficult to be completely separated without sacrificing one or another to soluble fragments, it is advantageous and economic to use this lignin/hemicelluloses mixture together as a carbon source, while sodium salts already present could serve as the activating agents to produce porous structures without needing further addition of chemicals. The KOH dissolution stream from $NaClO_2$-treated rice straw should contain mainly potassium silicate, which may serve as a precursor to silica. These precursors in both streams would be recovered by precipitation using ethanol for lignin/hemicelluloses carbon precursors and acidified poly(ethylene oxide) for the silica precursors. These two precursors could be thermally converted to carbon and silica products via a single-step pyrolysis and calcinations at 800 and 500 °C, respectively.

## ■ EXPERIMENTAL DETAILS

**Chemicals.** Rice straw (Calrose variety) used in this study was from the 2009 harvest in the Sacramento valley in northern California. Toluene ($C_6H_5CH_3$, ACS grade, Fisher Scientific), ethanol ($CH_3CH_2OH$, anhydrous, histological grade, Fisher Scientific), sodium chlorite ($NaClO_2$, 80%, Fluka), glacial acetic acid ($CH_3COOH$, 99.7%, ACS GR, EMD), poly(ethylene oxide) (PEO) ($M_w$ = 600 kDa, Sigma-Aldrich), and potassium hydroxide (KOH, 85%, EM Science) for fractionating rice straw components were used as received. Water used was purified by a Milli-Qplus water purification system (Millipore Corporate, Billerica, MA). All concentration and yield percentage values were based on weight unless otherwise specified.

**Preparation of Activated Carbon and Silica Particles from Rice Straw.** Fractional extraction of lignin/hemicelluloses and silica from rice straw was first performed by the $NaClO_2$ treatment as shown in Figure 1. Rice straw was washed thoroughly with water to rid of dirt, dried, and then milled (Thomas-Wiley Laboratory Mill model 4, Thomas Scientific, U.S.A.) to pass through mesh 60. Rice straw powders were Soxhlet extracted with 2:1 toluene/ethanol (v/v) at 55 °C for 24 h to remove all lipophilic and hydrophilic nonstructural components (Figure 1). The dewaxed rice straw powder was placed in 1.4 wt % $NaClO_2$ under acidic condition (pH ∼5 adjusted by 10% acetic acid) at a 15 mL/g liquid-to-solid ratio at 70 °C for 6 h and filtered to yield holocellulose/silica and filtrate 1. α-Cellulose was isolated from holocellulose by extracting with 5 wt % KOH at a 20 mL/g liquid-to-solid ratio at 70 °C for 24 h to give pure cellulose and dissolved silica and hemicelluloses in filtrate 2. Both filtrate 1 and 2 were then concentrated by heating at 90 °C to half their volumes. The remaining filtrates 4 and 5 contained mostly water with very little solutes. Ethanol in filtrate 4 may be recovered by distillation.

**Preparation of Activated Carbon.** Ethanol was added to the concentrated filtrate 1 at 3 times its volume to precipitate alkali-soluble lignin together with some hemicelluloses (LH). The LH powders were dried in oven at 60 °C for 12 h, placed in a quartz tube (2 cm inner diameter), and then pyrolyzed in a furnace (Mini-Mite, Lindberg/ Blue) at 10 °C/min to 105 °C and held for 0.5 h. Then the LH

B

dx.doi.org/10.1021/sc5000539 | ACS Sustainable Chem. Eng. XXXX, XXX, XXX−XXX

143 powders were heated to 800 °C and held for up to 0.5 h, all under
144 flowing N₂ at 100 mL/min. Finally, they were cooled to ambient
145 temperature in 12 h. The particles were washed with 5% HCl and
146 water to remove residual salts and other small hydrocarbon impurities
147 and then dried at 105 °C for 0.5 h to yield activated carbon (AC).

148 **Preparation of Silica Particles.** Acidified PEO solutions at 0.2%,
149 0.35%, 0.5%, and 1% were prepared by dissolving 0.04, 0.07, 0.1, and
150 0.2 g of PEO, respectively, in 20 g of 2% HCl and stirred for 6 h.
151 Concentrated filtrate 2 was added slowly to each acidified PEO
152 aqueous solution to form a milky white mixture and centrifuged
153 (Centrifuge 5804R, Eppendorf) at 5000 rpm for 15 min. The
154 precipitate was then washed with water thoroughly and dried in a
155 desiccator as silica and lignin/hemicelluloses/PEO (SHLP). The dried
156 SHLP powder was placed in a quartz tube (2 cm inner diameter) and
157 calcinated under flowing air (100 mL/min) in a furnace (Mini-Mite,
158 Lindberg/Blue). The sample was heated at 10 °C/min to 105 °C and
159 then 500 °C; the sample was held for 0.5 h at each temperature. The
160 obtained silica after calcination was cooled under flowing air (100 mL/
161 min) to room temperature in 12 h. Filtrate 4, SHLP, and silica were
162 referred to those obtained at 0.35% PEO unless stated otherwise.

163 **Analytical Methods.** The yields were calculated by the percentage
164 of extract or product mass over the original rice straw mass, both 0.1
165 mg accuracy (BP 300S, Satorius). The aqueous filtrates from the
166 extraction process were examined by ultraviolet−visible spectroscopy
167 (UV−vis) (Evolution 600, Thermo Scientific). UV samples were
168 placed in polystyrene cuvettes with a 1 cm path length. The chemical
169 composition and structure of LH, AC, SHLP, and silica were analyzed
170 by Fourier transform infrared spectroscopy (FTIR) (Nicolet 6700,
171 Thermo Scientific). All FTIR spectra were collected from samples
172 dried at 60 °C for 12 h and pressed with anhydrous KBr powders into
173 pellets. The elemental analysis of LH, AC, SHLP, and silica were
174 carried out by energy-dispersive X-ray spectroscopy (EDX) adjunct to
175 a scanning electron microscope (SEM) (FEI-XL 30, FEI). All samples
176 are stored in oven at 60 °C for 24 h before EDX measurements.

177 The morphology and structure of LH and SHLP as well as their
178 pyrolyzed products AC and silica were observed by SEM (FEI-XL 30,
179 FEI). The SEM samples were sputter coated with gold for 2 min and
180 then observed under a working voltage of 5 kV. The structures of AC
181 and silica particles were also examined by transmission electron
182 microscopy (TEM) (JEOL 3000, JEOL). TEM samples were prepared
183 by dispersing a small amount of AC and silica particles in water (~0.01
184 g/L) and sonicated (2510, Branson) for 60 min first, and then a drop
185 of the sonicated suspension was placed onto a carbon grid and dried in
186 air.

187 The thermal properties of LH and SHLP were analyzed by
188 differential scanning calorimetry (DSC) (DSC-60, Shimadzu) and
189 thermogravimetric analysis (TGA) (TGA-50, Shimadzu). DSC
190 samples were tightly packed in aluminum cells with press-sealed lids,
191 while TGA samples were placed in a platinum pan. LH samples were
192 heated to 60 °C and held for 2 h, then heated to 105 °C and held for
193 0.5 h, and finally heated to 550 and 800 °C for DSC and TGA,
194 respectively, and held for 0.5 h under 50 mL/min nitrogen flow. SHLP
195 samples were heated to 105 °C and held for 0.5 h and then heated to
196 500 °C and held for 0.5 h under a 50 mL/min air flow.

197 For surface area and pore characteristics, LH, AC, SHLP, and silica
198 were dried in oven at 50 °C for 48 h and then measured at 77 K by a
199 nitrogen adsorption−desorption analyzer (ASAP 2020, Micrometics).
200 The surface area was calculated from the isotherm using the
201 Brunauer−Emmett−Teller (BET) equation in the linear region
202 where relative pressure $P/P_0$ ranged from 0.05 to 0.1. The mesopore
203 surface areas of LH, AC, SHLP, and silica were derived from the
204 adsorption branch, whereas pore- and neck-size distributions were
205 derived from both adsorption and desorption branches of the isotherm
206 using the Barret−Joyner−Halenda (BJH) method. The micropore
207 surface area and pore hydraulic diameter distribution (0.7−1.6 nm) of
208 AC were derived from the t-plot using the Mikhail, Brunauer, and
209 Bodor MP method[29] and the Harkins and Jura equation.[30] Micropore
210 volume ($V_{mp}$) was derived from the tangent line of a contiguous range
211 of t-plots using the surface area of the filled pores via eq 1,

$$V_{mp} = \frac{(S_n - S_{n+1}) \times (t_n + t_{n-1})}{2} \times 15.47$$

(1)

212 where $S_n$ and $t_n$ are the surface area derived from the slope of tangent
213 and the thickness of absorbed layer at the $n$ point in the t-plot,
214 respectively, and 15.47 was the constant of converting the gas volume
215 to liquid volume at STP.
216

## RESULTS AND DISCUSSION

217 **Yields and Efficiency of Sodium Chlorite Isolation.** The
218 NaClO₂−KOH process for isolating rice straw components
219 involved three steps, yielding pure cellulose as well as filtrates 1
220 and 2 (Figure 1a). The washed and dried rice straw was
221 refluxed in a 2:1 toluene/ethanol (v/v) ratio at 55 °C for 24 h
222 to yield 94.7% dewaxed rice straw and a green-yellow distillate
223 containing surface oils, pigments, and possibly organic soluble
224 lignin. The dewaxed rice straw was then treated by 1.4%
225 NaClO₂ at pH 5 adjusted by acetic acid at 70 °C for 6 h and
226 then 5% KOH at 70 °C for 24 h to obtain pure cellulose as well
227 as the NaClO₂ and alkaline dissolution streams, that is, filtrates
228 1 and 2, respectively. Adding ethanol to filtrate 1 under the
229 basic condition precipitated the dissolved lignin/hemicelluloses
230 (LH) at 5.7% of the original rice straw mass (Figure 1b).
231 Adding the basic filtrate 2 to the dilute acidified PEO
232 precipitated silica along with remaining lignin/hemicellulose
233 (SHLP) at similar yields of 22.1−23.7%, increasing to 0.2−1%
234 PEO concentrations (Figure 1c). At 0.35% PEO, the silica/
235 hemicelluloses/lignin (SHL) yield was 20.7%, assuming all
236 PEO precipitated.
237

238 **Chemical Structures of Extracts and Final Products.**
239 NaClO₂ and KOH treatments yielded respective filtrates 1 and
240 2, which were precipitated as precursors to be subsequently
241 converted to AC and silica particles, respectively. The
242 compositions and structures of both filtrates, their precipitates,
243 and final products were examined by UV−vis, FTIR, and
244 elemental analysis to determine their compositions and to
245 assess the isolation process.

246 **UV−Vis Spectra of the Filtrates.** The UV−vis spectrum
247 of filtrate 1 exhibited strong broad absorbance below 300 nm
248 (Figure 2), ascribing to partially oxidized and/or decomposed
249 lignin from NaClO₂, possibly a polylignol dehydrogenative
250 copolymer of sinapyl alcohol, coniferyl alcohol, p-coumaryl
251 alcohol, and hydroxycinnamic acid esters.[31,32] Filtrate 2 showed
252 reduced yet clear UV absorbance below 300 nm, indicating the
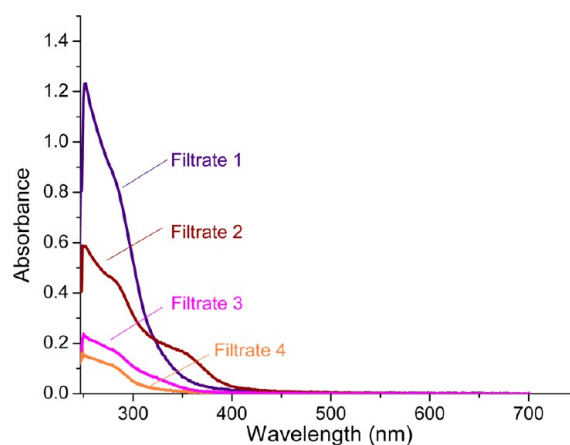


**Figure 2.** UV−vis spectra of filtrates from rice straw isolation shown in Figure 1.

C

dx.doi.org/10.1021/sc5000539 | ACS Sustainable Chem. Eng. XXXX, XXX, XXX−XXX

presence of some alkaline-soluble lignin and incomplete lignin removal in the previous NaClO$_2$ step. The broad absorption peak in the 360 nm region of the filtrate 2 spectra is consistent with the expected alkaline-soluble lignin, possibly various lignin derivatives of o,p-dihydroxystilbenes, $\alpha$-carbonyl phenolics, esters of p-coumaric, and ferulic acids,[33] as well as charge−transfer complexes from the carbonyl and carboxyl-conjugated heteroaromatic compounds.[34] Filtrate 3 showed very little absorbance below 300 nm, indicating effective precipitation of lignin in LH by ethanol. Filtrate 4 also exhibited reduced peak intensity below 300 nm, showing the presence of a small amount of alkaline-soluble lignin in this final filtrate. The UV−vis spectrum suggested that most lignin in rice straw was extracted by NaClO$_2$ dissolution in filtrate 1 and recovered by ethanol precipitation in LH, while some lignin present in the alkaline filtrate 2 was mostly precipitated by PEO in SHLP, leaving yet a small residual lignin in filtrate 4. Therefore, lignin in rice straw was recovered by precipitation mainly in LH from filtrate 1 and partially in SHLP from filtrate 2, with a residual amount in the final filtrate 4.

**FTIR Spectra of Precipitates and Final Products.** The FTIR spectrum of the LH precipitate from filtrate 1 showed major lignin characteristic peaks, including those between 1600 and 1000 cm$^{-1}$ from partially oxidized phenylpropanoids and multiple hydroxyl peaks (Figure 3). Lignin was evident by the

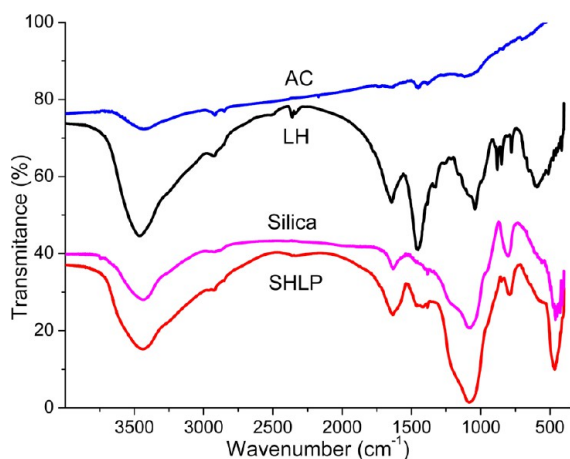**Figure 3.** FTIR spectrum of LH, AC, SHLP, and silica.

strong 1450 and 1040 cm$^{-1}$ peaks associated with aromatic C=C stretching and aromatic =C−H in-plane bending, respectively. The prominent peak at 3459 cm$^{-1}$ and two minor peaks at 2930 and 2835 cm$^{-1}$ were attributed to OH stretching in the respective hydrogen-bonded and free hydroxyls, whereas the ones at 1090 cm$^{-1}$ were from C−O deformation in the aliphatic hydroxyl and ether groups. The broad band at 1630 cm$^{-1}$ could be from moisture peaks overlapped with various C=O stretching, C=C stretching in phenylpropanoid side chains, and aromatic skeleton vibration. Therefore, LH precipitated from filtrate 1 consisted mainly of oxidized lignin from reaction with the strongly oxidative NaClO$_2$.

SHLP precipitated from filtrate 2 with diluted PEO showed characteristic peaks of silica, lignin, hemicelluloses, and PEO (Figure 3). Silica was clearly evident by the prominent Si−O−Si asymmetric and symmetric stretching peaks at 1090 and 460 cm$^{-1}$, respectively, as well as a Si−O deformation peak at 795 cm$^{-1}$. The presence of lignin was evident by the benzene C=C stretching peak at 1460 cm$^{-1}$. However, the peak intensity

decreased greatly compared to that of LH, suggesting the reduced lignin composition in SHLP. The broad shoulder at 1205 cm$^{-1}$ was ascribed to the various C−O−C stretching from hemicelluloses and PEO. The broad shoulder at 1640 cm$^{-1}$ was from moisture overlapping with C=C stretching and various esters and ketone structures, such as $\beta$ ketone ester, $\alpha-\beta$ unsaturated ketone, and $\beta$ diketone (enol form) in hemicelluloses. The broad 3430 cm$^{-1}$ peak as well as minor peaks at 2930 and 2835 cm$^{-1}$ were ascribed to hydroxyls from moisture, lignin/hemicelluloses, and silica surfaces.

The pyrolytic product of LH from heating at 800 °C showed little characteristic FTIR peaks of either lignin or hemicelluloses as expected. The broad OH stretching peak around 3440 cm$^{-1}$ greatly decreased in intensity compared to LH, clearly showing the loss of hydroxyls and is consistent with transformation of hydrophilic lignin/hemicelluloses to hydrophobic carbon. The only two small peaks at 1454 and 1380 cm$^{-1}$ were ascribed to aliphatic C−H bending. Thus, the FTIR of pyrolyzed LH is consistent with conversion to carbon with few lignin and hemicelluloses features.

The FTIR spectrum of SHLP calcinated at 500 °C showed only silica characteristic peaks, that is, Si−O−Si asymmetric and symmetric stretching at 1080 and 460 cm$^{-1}$, respectively, and Si−O deformation at 780 cm$^{-1}$, as well as the broad hydroxyl stretching peaks at 3440 and 1630 cm$^{-1}$, indicating absorbed moisture or the hydrophilic nature of silica. None of the lignin, hemicelluloses, and PEO characteristic peaks was observed, confirming their removal upon calcination.

UV−vis results clearly showed that lignin-rich LH and silica/hemicelluloses-rich SHLP were successfully isolated in filtrates 1 and 2, respectively, while FTIR confirmed that the isolated lignin in LH and hemicelluloses in SHLP were oxidized and degraded by the oxidative NaClO$_2$ and then thermally converted to carbon and silica, respectively.

**Elemental Analysis of Extracts.** The elemental compositions by EDX show LH to consist of 38.0% C, 42.8% O, 18.6% Na, and 0.6% Si (Table 1). The high Na and O contents

**Table 1. Elemental Compositions (wt%) of Crude LH and SHLP and Their Respective Pyrolyzed Products: AC (800 °C, 30 min) and Silica (500 °C, 0.5 h)**

|        | C    | O    | Si   | Na   |
|--------|------|------|------|------|
| LH     | 38.0 | 42.8 | 0.6  | 18.6 |
| AC     | 81.7 | 15.8 | 2.5  | 0    |
| SHLP   | 16.6 | 51.7 | 29.7 | 0    |
| silica | 0    | 53.0 | 47.0 | 0    |

suggested LH contained oxy-salts of sodium, possibly sodium carbonates, oxidative products of lignin/hemicelluloses, and acetic acid in the NaClO$_2$ step. The continuous evolution of odorless bubbles when adding crude LH powder into dilute aqueous HCl indicated gaseous products and was consistent with the presence of carbonate salts in crude LH. To further investigate the compositions of inorganic salts, LH was calcinated at 500 °C for 6 h. The yellow color of LH turned to a white color after calcination (Figure S1, Supporting Information) and was shown by EDX to have the elemental composition of Na$_2$CO$_3$ (Figure S1, Supporting Information), confirming the presence of sodium carbonates in crude LH. As LH was precipitated from aqueous solution, sodium carbonate should exist in the form of monohydrate after drying at 60 °C. Under this assumption, monohydrate sodium carbonate
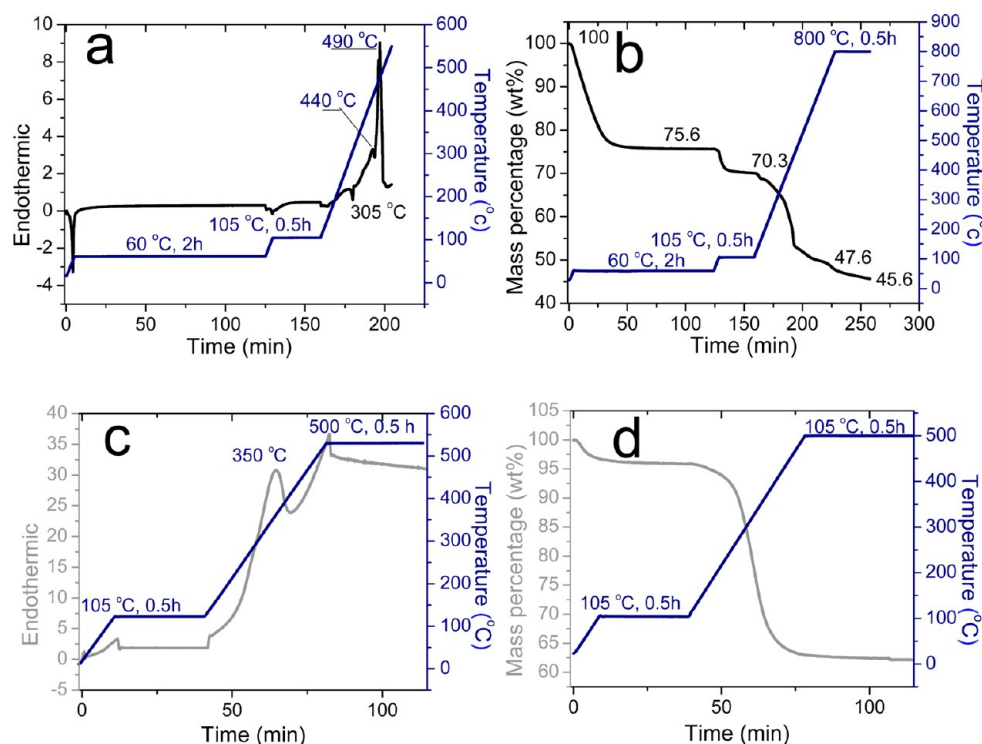
**Figure 4.** Thermal characteristics of crude LH (a,b) and SHLP (c,d): (a,c) DSC and (b,d) TGA thermographs.

content in the crude LH precipitate would be 50.1%, leaving 49.9% to be lignin and hemicelluloses (LH). Such a unique composition allowed LH to be directly pyrolyzed into AC, without the need to add additional activating chemicals, making this pathway superior than previously reported approaches.[16−18] SHLP consisted of 16.6% C, 51.7% O, and 29.7% Si, showing its elemental compositions to be mainly silica (64%) and lignin/hemicelluloses/PEO (36%). This three-step toluene/ethanol, NaClO$_2$, and KOH isolation process isolated 5.3% waxes and organic extracts, 36% highly pure cellulose,[3] 2.8% LH, and 20.7% SHL, or 65% of precursors, leaving about 35% rice straw components as soluble from NaClO$_2$ oxidation and KOH dissolution in the remaining filtrates.

The chars pyrolyzed from LH after dilute HCl washing consisted of 81.7% C, 15.8% O, and 2.5% Si, confirming substantial carbon with little silica impurities. After calcinating SHLP at 500 °C for 0.5 h, only 47% Si and 53% O were detected, while no carbon was present. This mass percentage is equivalent to a 1:2 Si/O atomic ratio or that of pure silica.

**Thermal Properties of Extracts.** The thermograms of LH showed a very sharp exothermic peak at 60 °C and a small exotherm around 105 °C (Figure 4a) with respective 24.4% and 5.3% mass losses (Figure 4b), reflecting the transition from sodium carbonate decahydrate to monohydrate as well as moisture loss from lignin and hemicelluloses. The endotherm at 300 °C is attributed to the decomposition of hemicelluloses, while two exotherms at 430 and 475 °C were likely from decomposition and further charring of lignin, corresponding to the major 19.2% mass loss, that is, from 70.7% at 105 °C to 51.5% at 550 °C. The solid mass was lowered to 47.6% when heated to 800 °C initially and slightly lowered to 45.6% when held for additional 30 min.

The thermal analysis further supported the compositions derived from EDX that the crude LH at ambient temperature was a mixture of sodium carbonate monohydrate and decahydrate as well as lignin/hemicelluloses. Assuming the mass loss at 105 °C is solely caused by the transformation of sodium carbonate monohydrate to the anhydrous form, the weight percentages of sodium carbonate monohydrate and Na in crude LH were estimated to be 48.3% and 17.9%, respectively (eqs 1 and 2), very close to the 50.1% estimated from EDX elemental analysis. These values are slightly higher than the atomic compositions due to the missing hydrogen in the EDX. The composition of crude LH precipitate at 105 °C would thus be estimated to be 44.4% anhydrous sodium carbonate and 55.6% lignin/hemicelluloses (eq 3). Therefore, the final pyrolyzed product could be a mixture of lignin char and various forms of sodium, sodium carbonate, sodium oxide, and elementary sodium, all of the latters removed in the wash to obtain 1.3% activated carbon (AC) from the starting rice straw.

SHLP showed an endothermic shoulder below 105 °C (Figure 4c) accompanied by a slight 4% mass loss from moisture (Figure 4d). A broad exothermic peak centered at 350 °C was observed along with a significant 33% mass loss, that is, from 96% at 105 °C to 63% at 500 °C, due to thermal decomposition of hemicelluloses/lignin/PEO. This quantity was consistent with the 64% silica from the EDX analysis. When held at 500 °C for 0.5 h, the DSC thermograph baseline shifted endothermically, while the solid mass slightly decreased from 63% to 61.5%, indicating further combustion of the residual carbon char, obtaining 14% pure silica from the starting rice straw.
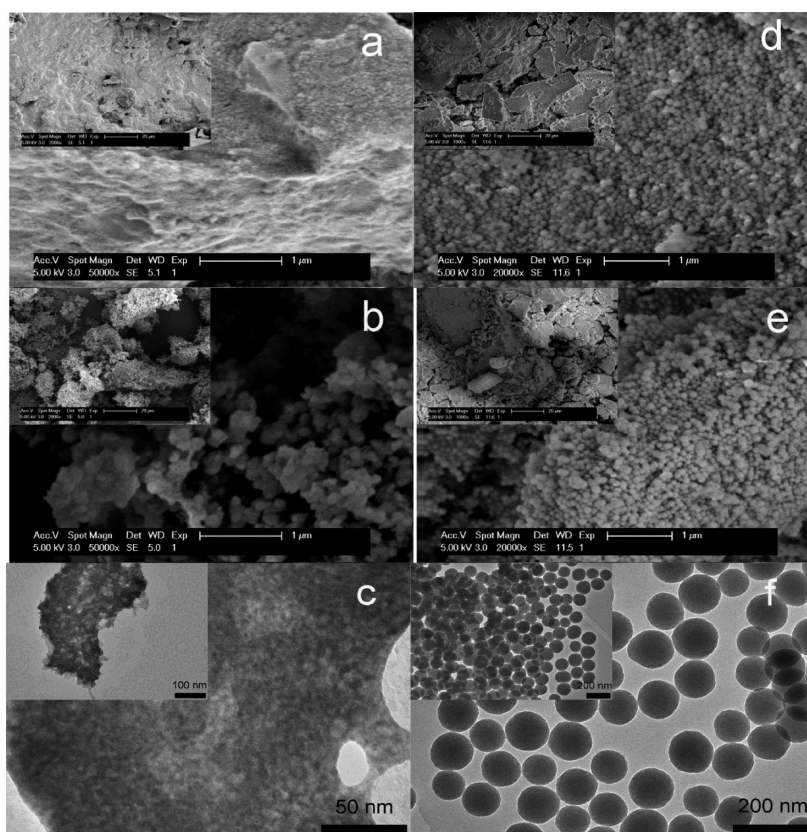
**Figure 5.** SEM (a,b,d,e) and TEM (c,f) of (a) LH, (b,c) AC, (d) SHLP, and (e,f) silica. Insets in SEM: scale bar = 20 $\mu$m.

$$\text{Na}_2\text{CO}_3 \bullet \text{H}_2\text{O}_{(\text{at } 60 \,^\circ\text{C})} \, (\text{wt\%}) = \frac{\text{Mass loss from Na}_2\text{CO}_3 \bullet \text{H}_2\text{O to Na}_2\text{CO}_3 \, (\text{wt\%}) \times \text{Molar mass of Na}_2\text{CO}_3 \bullet \text{H}_2\text{O}}{\text{Molar mass of H}_2\text{O} \times \text{Mass percentage of solid residue}_{(\text{at } 60 \,^\circ\text{C})}} = \frac{5.3 \, \text{wt\%} \times 124}{18 \times 0.756} = 48.3 \, (\text{wt\%}) \tag{1}$$

$$\text{Na}_{(\text{at } 60 \,^\circ\text{C})} \, (\text{wt\%}) = \text{Na}_2\text{CO}_3 \bullet \text{H}_2\text{O}_{(\text{at } 60 \,^\circ\text{C})} \, (\text{wt\%}) \times \frac{\text{Molar mass of Na} \times 2}{\text{Molar mass of Na}_2\text{CO}_3 \bullet \text{H}_2\text{O}} = 48.3 \times \frac{46}{124} = 17.9 \, (\text{wt\%}) \tag{2}$$

$$\text{Na}_2\text{CO}_{3(\text{at } 60 \,^\circ\text{C})} \, (\text{wt\%}) = \text{Na}_2\text{CO}_3 \bullet \text{H}_2\text{O}_{(\text{at } 60 \,^\circ\text{C})} \, (\text{wt\%}) \times \frac{\text{Molar mass of Na}_2\text{CO}_3}{\text{Molar mass of Na}_2\text{CO}_3 \bullet \text{H}_2\text{O}} = 48.3 \times \frac{106}{124} = 41.3 \, (\text{wt\%}) \tag{3}$$

$$\text{Na}_2\text{CO}_{3(\text{at } 60 \,^\circ\text{C})} \, (\text{wt\%}) = \frac{\text{Na}_2\text{CO}_{3(\text{at } 60\,^\circ\text{C})} \, (\text{wt\%})}{\text{Na}_2\text{CO}_{3(\text{at } 60\,^\circ\text{C})} \, (\text{wt\%}) + (100 - \text{Na}_2\text{CO}_3 \bullet \text{H}_2\text{O}_{(\text{at } 60\,^\circ\text{C})} \, (\text{wt\%}))} \times 100 = \frac{41.3}{41.3 + 100 - 48.3} \times 100 = 44.4 \, (\text{wt\%}) \tag{4}$$

On the basis of the TGA analysis, the LH component contained 51% sodium salt or about 2.8% yield of lignin/hemicelluloses from NaClO$_2$ dissolution of rice straw (e.g., filtrate 1). SHLP consisted of 61.5% silica, 29.3% lignin/hemicelluloses, and 9.2% PEO or 14% silica and 6.7% lignin/hemicelluloses yields from the KOH dissolution stream (e.g., filtrate 2). From these and our prior report on cellulose,[3] this three-step toluene/ethanol acidic NaClO$_2$–KOH process has shown to isolate 5.3% waxes and organic extracts, 36%

celluloses, 9.5% lignin/hemicelluloses, and 14% silica from rice straw, that is, 65% of rice straw. The lignin/hemicelluloses and silica were eventually converted to 1.3% AC and 14% pure silica.

**Surface and Morphology of Activated Carbon and Silica.** The LH powders were gray in color and appeared as packed particulates in over 20 $\mu$m sizes (Figure 5a). After pyrolysis at 800 °C for 30 min, the obtained AC appeared as irregularly shaped porous clusters of 100–500 nm-sized

F

dx.doi.org/10.1021/sc5000539 | ACS Sustainable Chem. Eng. XXXX, XXX, XXX–XXX
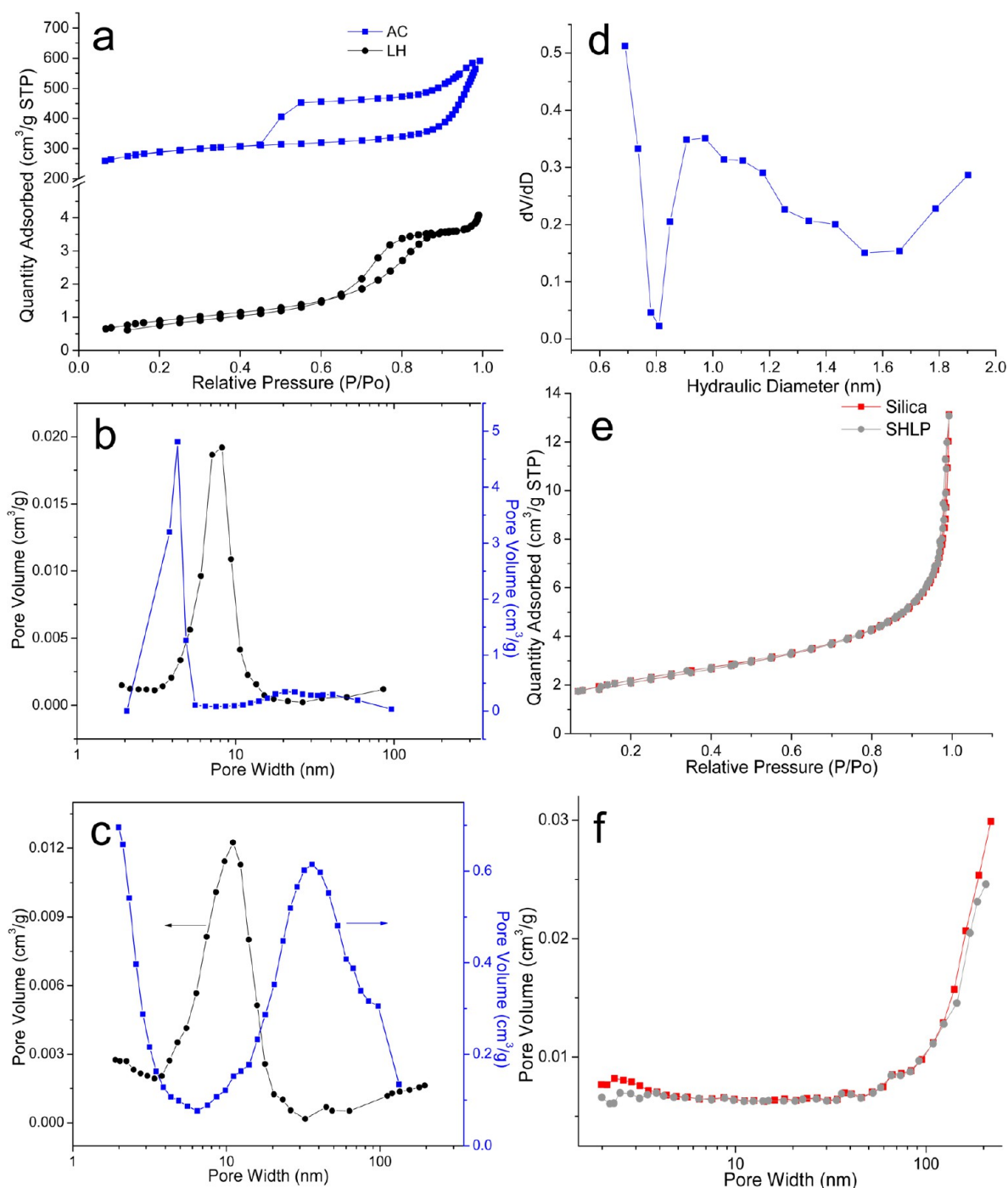
**Figure 6.** Nitrogen adsorption−desorption isotherms of (a,b,c,d) of LH and AC (800 °C, 0.5 h, N₂) and (e,f) SHLP and silica (500 °C, 0.5 h, air): (a,e) isotherm, (b) BJH neck-size distribution, (c,f) BJH pore/cavity width distribution, and (d) micropore hydraulic diameter distribution.

particles (Figure 5b), which are much smaller than the ACs in the previous studies.[16−18] These much shorter diffusion lengths contribute to faster adsorption rate, which is a desirable property of AC absorbent. The TEM images showed the semi-crescent AC particles had about a 450 nm Feret diameter. The randomly distributed slit-shaped micropores and small mesopores were observed within the particle (Figure 5c). Such porosity was generated by sodium carbonate activation as well as pyrolytic decomposition of hemicelluloses and removal of sodium byproducts from washing.

The SEM showed smaller and more narrowly distributed SHLP particles with increasing PEO concentrations (Figure S2, Supporting Information). Semi-spherical particles from 100 to 200 nm sizes were obtained at 0.2% PEO. With increasing PEO concentrations to 0.35%, more uniformly sized nanospheres between 100 and 150 nm were formed (Figure 5d−f), possibly due to better capping of particles preventing them from aggregating and/or growing into larger particles. At 0.5 wt % PEO and above, however, the particles became irregularly shaped and polydispersed in sizes less than 50 nm, possibly from easy sintering during calcination. Only the SLHP particles precipitated from 0.35% acidified PEO remained similar in size after calcinations. Such a PEO precipitation approach has proven to be fast and effective, without the need for the time-

G

**Table 2. Physical Properties of LH, AC, SHLP, and Silica Deduced from $N_2$ Adsorption−Desorption at 77 K**

| | BET surface area $(m^2/g)$ | BJH adsorption cumulative surface area between 1.7 and 300 nm width $(m^2/g)$ | single-point desorption pore volume $(cm^3/g)$ | BJH adsorption cumulative volume of pore between 1.7 and 300 nm $(cm^3/g)$ | t-plot-derived micropore surface area between 0.7 and o 2 nm width $(m^2/g)$ | t-plot-derived micropore volume $(cm^3/g)$ |
|---|---|---|---|---|---|---|
| LH | 3 | 3 | 0.006 | 0.006 | 0 | 0 |
| AC | 997 | 249 | 0.90 | 0.58 | 592 | 0.27 |
| SHLP | 7.9 | 6.6 | 0.015 | 0.020 | 0 | 0 |
| silica | 7.2 | 6.1 | 0.014 | 0.019 | 0 | 0 |

consuming aging process. The obtained silica spheres were much more uniform in both size and shape than those previously reported.[17,20] The high size uniformity is crucial to fine-tune the properties of silica particles to be used as additive/fillers for composites or further functionalized for other applications.

**Porous Structure of Activated Carbon and Silica.** The as-prepared LH powders appeared flaky and showed a H2 hysteresis in a BET nitrogen adsorption isotherm (Figure 6a) with a very low surface area of 3 $m^2/g$ and a pore volume of 0.006 $cm^3/g$, indicative of their nonporous nature (Table 2). The extremely low surface area was attributed to secondary porosity, for example, interparticulate mesopores distributed between 3 and 30 nm, and peaked at 10 nm as shown in the pore width distribution (Figure 6b). Carbonization at 800 °C for 30 min significantly increased the BET surface area of the submicrometer-sized AC particles to 997 $m^2/g$ and total pore volume to 0.9 $cm^3/g$, that is, a specific surface area over 330 times of that of the LH precursor. The BJH surface area and pore volume of the meso/macropores between 1.7 and 300 nm were estimated to be 249 $m^2/g$ and 0.58 $cm^3/g$, respectively, and those of the t-plot-derived micropores below 2 nm were approximated to be 592 $m^2/g$ and 0.27 $cm^3/g$, respectively (Table 2) Therefore, the surface area was mostly attributed to the micropores, while the pore volume was attributed to the larger mesopores and macropores. The type IV isotherm with noticeable H4 hysteresis observed on AC (Figure 6a) suggests a slit-like micro/mesoporous structure.[35] The micropores ranged from 0.8 to 1.6 nm in diameter, peaking at 0.95 nm (Figure 6d), whereas the mesopores were bimodally distributed between 2 and 6 nm as well as between 10 nm to submicrometer (Figure 6c), consistent with TEM observations (Figure 5c). The adsorption−desorption isotherms exhibited characteristic step-down at 0.45 $P/P_0$, while the pore width distribution derived from the desorption branch showed a distinct peak around 4 nm from cavitation of nitrogen during desorption (Figure 6b), indicating mesopores connected by slit-like micropores consistent to similar observations by others.[36,37] The internal micropores and mesopores contributed mostly to the high surface area and pore volume of AC, while the large macropores likely from interparticle spacing (secondary porosity) as shown in the SEM (Figure 5b) contributed little.

Both SHLP and silica exhibited type II BET nitrogen adsorption isotherms, typical of nonporous and macroporous materials with weak affinities to nitrogen (Figure 6e). Both had very similarly low BET surface area and pore volume of about 7 $m^2/g$ and 0.015 $cm^3/g$, respectively, as well as BJH mesoporous surface area and pore volume of about 6 $m^2/g$ and 0.002 $cm^3/g$, respectively (Table 2). Only macropores larger than 100 nm were observed in both (Figure 6f). There was no evidence of mesopores. These observations were consistent with their low surface areas and pore volume that were mainly attributed to the external particle surfaces and interparticulate spacing. In calcination of SHLP, the organic hemicelluloses, lignin, and PEO components were removed, leaving only silica with no porosity as indicated by the nitrogen adsorption−desorption analysis. This nonporous structure suggests that the organic components are either mainly capped on the silica particle surface and/or well mixed with silica to create micropores that collapse during calcinations or are below the 0.3 nm nitrogen adsorption−detection level of the instrument used.

## CONCLUSION

This study has demonstrated the feasibility to optimally isolate the lignin, hemicellulose, and silica components from rice straw, along cellulose previously reported,[3] and efficiently convert them into advanced materials. An efficient three-step toluene/ethanol, $NaClO_2$, and KOH isolation process has been successfully devised for isolating two-thirds of crude rice straw into at least 36% pure cellulose from rice straw while generating two filtrates, 2.8% lignin-rich LH and 20.7% silica−hemicellulose-rich SHL as precursors for activated carbon and silica particles, respectively. The $NaClO_2$ dissolution stream from the dewaxed rice straw contains oxidized lignin and hemicelluloses as carbon precursors as well as sodium carbonates as activating chemicals that can be precipitated for direct carbonization at 800 °C to yield 1.3% activated carbon particles with submicrometer sizes between 100 and 500 nm as well as high specific surface area (997 $m^2/g$) and pore volume (0.90 $cm^3/g$). The KOH dissolution stream from $NaClO_2$-treated rice straw contains mainly potassium silicate and a small amount of lignin/hemicelluloses and could be precipitated by dilute (0.35%) acidified poly(ethylene oxide) and calcinated to yield 14% pure, nonporous, silica nanospheres in 100 to 120 nm diameters. This is the first report of highly efficient processes that optimally isolated and fully utilized all major rice straw components, the highest quantity agricultural crop byproduct in the world. Together with nanocellulose products reported,[3] 80% of the isolated components or 51.5% of crude rice straw was converted into high quality particulates of highly porous activated carbon particles and uniformly sized non-porous silica nanoparticles. These high quality nanomaterials can provide broadly available feedstock for advanced materials.

## ASSOCIATED CONTENT

**Ⓢ Supporting Information**

EDX of LH after calcination and SEMs of silica particles precipitated by acidified PEO of different concentrations before and after calcination. This material is available free of charge via the Internet at http://pubs.acs.org.

## AUTHOR INFORMATION

**Corresponding Author**

*E-mail: ylhsieh@ucdavis.edu.

**Notes**

The authors declare no competing financial interest.

## ■ REFERENCES

(1) Alonso, D. M.; Bond, J. Q.; Dumesic, J. A. Catalytic conversion of biomass to biofuels. *Green Chem.* **2010**, *12* (9), 1493−1513.

(2) Stocker, M. Biofuels and biomass-to-liquid fuels in the biorefinery: Catalytic conversion of lignocellulosic biomass using porous materials. *Angew. Chem., Int. Ed.* **2008**, *47* (48), 9200−9211.

(3) Wyman, C. E. Ethanol from lignocellulosic biomass − Technology, economics, and opportunities. *Bioresour. Technol.* **1994**, *50* (1), 3−16.

(4) Maschio, G.; Koufopanos, C.; Lucchesi, A. Pyrolysis, a promising route for biomass utilization. *Bioresour. Technol.* **1992**, *42* (3), 219−231.

(5) Datar, R.; Huang, J.; Maness, P. C.; Mohagheghi, A.; Czemik, S.; Chornet, E. Hydrogen production from the fermentation of corn stover biomass pretreated with a steam-explosion process. *Int. J. Hydrogen Energy* **2007**, *32* (8), 932−939.

(6) Lu, P.; Hsieh, Y. L. Preparation and characterization of cellulose nanocrystals from rice straw. *Carbohydr. Polym.* **2012**, *87* (1), 564−573.

(7) Alemdar, A.; Sain, M. Isolation and characterization of nanofibers from agricultural residues − Wheat straw and soy hulls. *Bioresour. Technol.* **2008**, *99* (6), 1664−1671.

(8) Tay, T.; Ucar, S.; Karagoz, S. Preparation and characterization of activated carbon from waste biomass. *J. Hazard. Mater.* **2009**, *165* (1−3), 481−485.

(9) Dodson, J. R.; Cooper, E. C.; Hunt, A. J.; Matharu, A.; Cole, J.; Minihan, A.; Clark, J. H.; Macquarrie, D. J. Alkali silicates and structured mesoporous silicas from biomass power station wastes: The emergence of bio-MCMs. *Green Chem* **2013**, *15* (5), 1203−1210.

(10) Mansour, N. A. L.; Hanna, S. B. Silicon-carbide and nitride from rice hulls 0.2. Effect of iron on the formation of silicon-carbide. *Trans. J. Br. Ceram. Soc.* **1979**, *78* (6), 132−136.

(11) FAOSTAT, 2011. Food and Agriculture Organization of the United Nations. http://faostat.fao.org/.

(12) Moo-Young, M., Ed.; *Comprehensive Biotechnology: The Principles, Applications, and Regulations of Biotechnology in Industry, Agriculture, and Medicine*; Pergamon Press: Oxford, U.K., 1985.

(13) Binod, P.; Sindhu, R.; Singhania, R. R.; Vikram, S.; Devi, L.; Nagalakshmi, S.; Kurien, N.; Sukumaran, R. K.; Pandey, A. Bioethanol production from rice straw: An overview. *Bioresour. Technol.* **2010**, *101* (13), 4767−4774.

(14) Huang, Y. F.; Kuan, W. H.; Lo, S. L.; Lin, C. F. Hydrogen-rich fuel gas from rice straw via microwave-induced pyrolysis. *Bioresour. Technol.* **2010**, *101* (6), 1968−1973.

(15) Reddy, N.; Yang, Y. Q. Properties of high-quality long natural cellulose fibers from rice straw. *J. Agric. Food Chem.* **2006**, *54* (21), 8077−8081.

(16) Basta, A. H.; Fierro, V.; Ei-Saied, H.; Celzard, A. 2-Step KOH activation of rice straw: An efficient method for preparing high-performance activated carbons. *Bioresour. Technol.* **2009**, *100* (17), 3941−3947.

(17) An, D. M.; Guo, Y. P.; Zou, B.; Zhu, Y. C.; Wang, Z. C. A study on the consecutive preparation of silica powders and active carbon from rice husk ash. *Biomass Bioenergy* **2011**, *35* (3), 1227−1234.

(18) Gao, P.; Liu, Z. H.; Xue, G.; Han, B.; Zhou, M. H. Preparation and characterization of activated carbon produced from rice straw by $(NH_4)_2HPO_4$ activation. *Bioresour. Technol.* **2011**, *102* (3), 3645−3648.

(19) Zaky, R. R.; Hessien, M. M.; El-Midany, A. A.; Khedr, M. H.; Abdel-Aal, E. A.; El-Barawy, K. A. Preparation of silica nanoparticles from semi-burned rice straw ash. *Powder Technol.* **2008**, *185* (1), 31−35.

(20) Hessien, M. M.; Rashad, M. M.; Zaky, R. R.; Abdel-Aal, E. A.; El-Barawy, K. A. Controlling the synthesis conditions for silica nanosphere from semi-burned rice straw. *Mater. Sci. Eng., B* **2009**, *162* (1), 14−21.

(21) Lu, P.; Hsieh, Y. L. Highly pure amorphous silica nano-disks from rice straw. *Powder Technol.* **2012**, *225*, 149−155.

(22) Patel, M.; Kumari, P. Silicon-carbide from sugarcane leaf and rice straw. *J. Mater. Sci. Lett.* **1990**, *9* (4), 375−376.

(23) Kadam, K. L.; Forrest, L. H.; Jacobson, W. A. Rice straw as a lignocellulosic resource: Collection, processing, transportation, and environmental aspects. *Biomass Bioenergy* **2000**, *18* (5), 369−389.

(24) Xiao, B.; Sun, X. F.; Sun, R. C. Chemical, structural, and thermal characterizations of alkali-soluble lignins and hemicelluloses, and cellulose from maize stems, rye straw, and rice straw. *Polym. Degrad. Stab.* **2001**, *74* (2), 307−319.

(25) Sangnark, A.; Noomhorm, A. Chemical, physical and baking properties of dietary fiber prepared from rice straw. *Food Res. Int.* **2004**, *37* (1), 66−74.

(26) Karimi, K.; Emtiazi, G.; Taherzadeh, M. J. Production of ethanol and mycelial biomass from rice straw hemicellulose hydrolyzate by *Mucor indicus*. *Process Biochem.* **2006**, *41* (3), 653−658.

(27) Kargbo, F. R.; Xing, J. J.; Zhang, Y. L. Pretreatment for energy use of rice straw: A review. *Afr. J. Agric. Res.* **2009**, *4* (13), 1560−1565.

(28) Jiang, F.; Hsieh, Y. L. Chemically and mechanically isolated nanocellulose and their self-assembled structures. *Carbohydr. Polym.* **2013**, *95* (1), 32−40.

(29) Mikhail, R. S.; Brunauer, S.; Bodor, E. E. Investigations of a complete pore structure analysis. I. Analysis of micropores. *J. Colloid Interface Sci.* **1968**, *26* (1), 45−&.

(30) Harkins, W. D.; Jura, G. An adsorption method for the determination of the area of a solid without the assumption of a molecular area, and the area occupied by nitrogen molecules on the surfaces of solids. *J. Chem. Phys.* **1943**, *11* (9), 431−432.

(31) He, L. F.; Terashima, N. Formation and structure of lignin in monocotyledons 0.4. Deposition process and structural diversity of the lignin in the cell-wall of sugarcane and rice plant studied by ultraviolet microscopic spectroscopy. *Holzforschung* **1991**, *45* (3), 191−198.

(32) Sun, R. C.; Tomkinson, J.; Mao, F. C.; Sun, X. F. Physicochemical characterization of lignins from rice straw by hydrogen peroxide treatment. *J. Appl. Polym. Sci.* **2001**, *79* (4), 719−732.

(33) Brauns, F. E. *The Chemistry of Lignin*; Academic Press: New York, 1952.

(34) Bikova, T.; Treimanis, A. UV-absorbance of oxidized xylan and monocarboxyl cellulose in alkaline solutions. *Carbohydr. Polym.* **2004**, *55* (3), 315−322.

(35) Seaton, N., Reinoso, F. R., Llewellyn, P., Kaskel, S., Eds.; *Characterisation of Porous Solids VIII. Proceedings of the 8th International Symposium on the Characterisation of Porous Solids*; RSC Publishing: London, 2009.

(36) Ravikovitch, P. I.; Neimark, A. V. Experimental confirmation of different mechanisms of evaporation from ink-bottle type pores: Equilibrium, pore blocking, and cavitation. *Langmuir* **2002**, *18* (25), 9830−9837.

(37) Thommes, M.; Smarsly, B.; Groenewolt, M.; Ravikovitch, P. I.; Neimark, A. V. Adsorption hysteresis of nitrogen and argon in pore networks and characterization of novel micro- and mesoporous silicas. *Langmuir* **2006**, *22* (2), 756−764.